

## Ocular Aberrations and their Measurement

Antonio Guirao<sup>\*,†</sup>, Donald T. Miller<sup>‡</sup>, David R. Williams<sup>\*,‡</sup>, Jason Porter<sup>\*,‡</sup>, and Yasuki Yamauchi<sup>\*</sup>

<sup>\*</sup> *Center for Visual Science, University of Rochester, Rochester, New York, 14627, USA*

<sup>†</sup> *Laboratorio de Optica, Universidad de Murcia, Campus de Espinardo (Edificio C), 30071 Murcia, SPAIN*

<sup>‡</sup> *School of Optometry, Indiana University, Bloomington, Indiana, 47405, USA*

<sup>‡</sup> *The Institute of Optics, University of Rochester, Rochester, New York, 14627, USA*

### 1. Introduction

As we described in the previous chapter, the first step in the visual process is the formation of an image on the retina by the eye's optics. Thus, the optical quality of the eye imposes the first limit on spatial vision (Charman, 1983). It has been long known that the normal human eye suffers from many aberrations that degrade retinal image quality (Helmholtz, 1896). As shown in Fig. 1, a point of light on the retina would emerge as a ideal, planar wavefront in a perfect eye. However, normal eyes possess optics with inferior quality, rendering a point source of light on the retina as an aberrated wavefront that exits the pupil of the eye. Hermann Von Helmholtz (1962) commented on the eye:

“ ... if an optician wanted to sell me an instrument which had all these defects, I should think myself quite justified in blaming his carelessness in the strongest terms, and giving him back his instrument.”

Spectacles and contact lenses have been successfully used to correct the eye's lower order aberrations (defocus and astigmatism or sphere, cylinder and axis). This conventional correction improves vision to an acceptable level. Until recently, defocus and astigmatism were the only aberrations that could be easily measured. Now, recent studies have found that higher order aberrations have a significant impact on retinal image quality, especially for large pupil sizes (Liang & Williams, 1997). Several accurate instruments now exist for measuring ocular aberrations.

Fig. 2 shows the effect of pupil size on the eye's point spread function (PSF), or how an observer would view a point source of light for two different pupil sizes. For the smaller pupil size of 2 mm, retinal image quality is mainly limited by diffraction (as illustrated by the Airy disk pattern in the PSF). However, aberrations become the dominant source of retinal image blur for large pupil sizes.

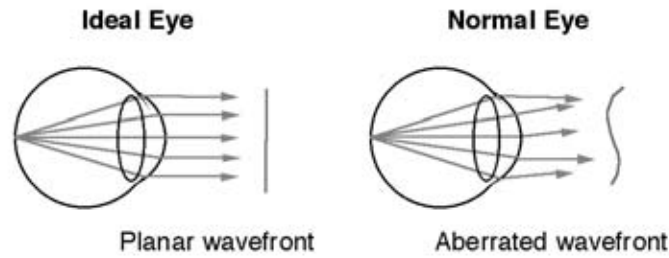


Figure 1. In an ideal eye, a point source on the retina yields parallel rays and a planar wavefront after the light passes through the eye's optics. In a normal eye, the wavefront exiting the eye is aberrated due to imperfections in the eye's optics.

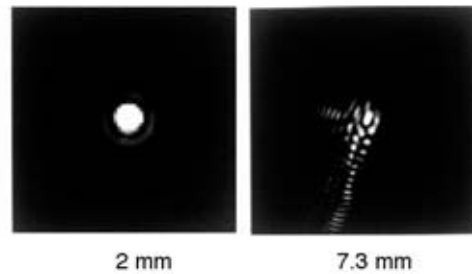


Figure 2. PSFs for a typical eye for 2 and 7.3 mm pupil diameters (as calculated from wave aberration measurements). Diffraction is the dominant source of image blur for small pupil sizes whereas aberrations are the major contributors to image degradation at large pupil sizes.

Improving the optics of the eye can improve vision up to the point where the eye's optical quality exceeds the limits set by the spacing between photoreceptors and subsequent neural factors (Williams, 1985). Fig. 3 shows the modulation transfer function (MTF) of the eye under normal viewing conditions for 3 and 7.3 mm pupil sizes, and the diffraction-limited MTF for the same pupil sizes. The areas between the curves, corresponding to the normal and diffraction-limited eyes, represent the range of contrast and spatial frequencies accessible by correcting the higher order aberrations.

## 2. History of Methods

Gullstrand was awarded the Nobel prize in 1911 for designing a schematic human eye used to model the optical properties inherent in a typical eye, shown in Fig. 4. His model eye consisted of spherical surfaces, and was sufficient to explain the refractive properties of the human eye in reasonable agreement with its

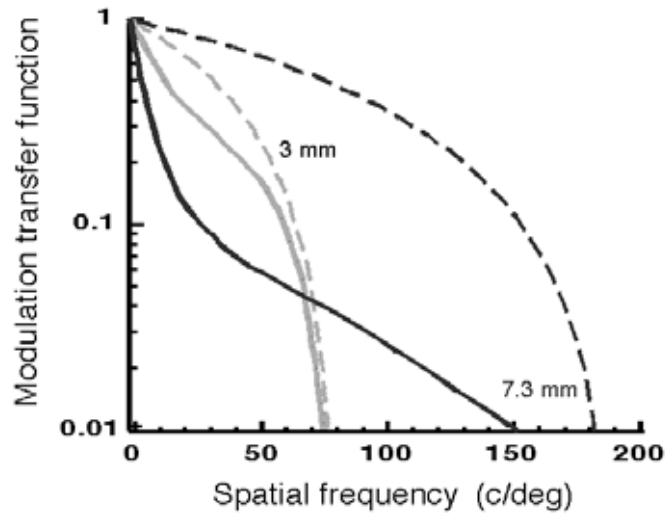


Figure 3. Average MTFs for the normal eye with the best refraction (solid) achievable using trial lenses for a 3 (gray lines) and 7.3 (black lines) mm pupil from 14 eyes (Miller, 2000). Diffraction limited curves for both pupil sizes are shown with dashed lines.

anatomy. Since then, many other schematic eyes have been proposed. The most sophisticated models have aspheric surfaces or gradient refractive index components that incorporate the effects of spherical aberration, but none of them can account for the effects of other higher order aberrations.

Several different techniques have been developed to measure the aberrations of the eye, including the double-pass method, the Smirnov technique, the interferometric method, and the aberroscope. The table below indicates when each method was first developed, whether the technique is objective or subjective, and the data measured: the modulation transfer function (MTF), the wave aberration (WA) or the point spread function (PSF).

Method	Year	Technique	Data
Double-Pass	1955	objective	PSF
Smirnov	1961	subjective	WA
Interferometric	1965	subjective	MTF
Aberroscope	1977	subjective/objective	WA
Hartmann-Shack	1994	objective	WA

### 2.1. Double-Pass method

The double-pass method is based on the recording of images of a point source projected on the retina after it reflects from the retina and passes back through the ocular media (shown in Fig. 5). The method was first proposed by Flament (1955) as a technique to estimate retinal image quality, and has undergone several technical innovations in recent years (Santamaría *et al.*, 1987): photo-multiplier tube, image intensifiers, and video cameras for capturing images; new

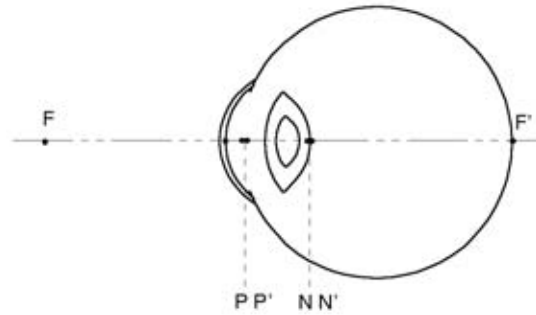


Figure 4. Gullstrand's schematic eye. N and N' are the nodal points, P and P' are the principal points, and F and F' are the eye's focal points.

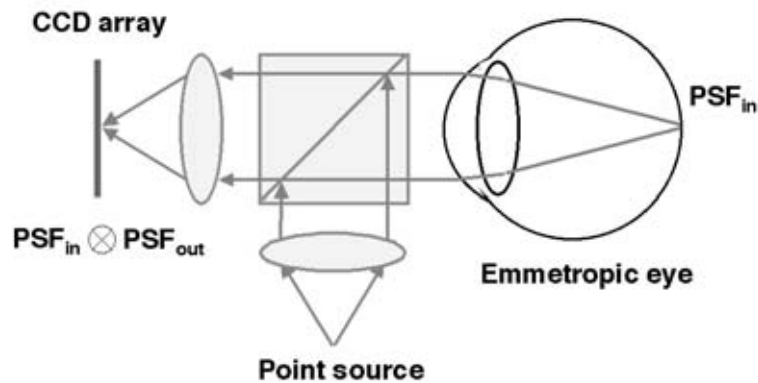


Figure 5. Double-pass method.

light sources for illumination, etc. This technique has provided relevant and widely used results on the eye's optical quality (Campbell & Gubisch, 1966; Navarro *et al.*, 1993; Artal & Navarro, 1994; Williams *et al.*, 1994; Williams *et al.*, 1996; Artal *et al.*, 1995a-b; Lopez-Gil *et al.*, 1998; Guirao & Artal, 1999; Guirao *et al.*, 1999).

Mathematically, the double-pass image is the autocorrelation of the PSF of the eye for the first pass with the PSF for the second pass (Artal *et al.*, 1995a). If both passes are symmetrical, the MTF can be calculated from the double-pass image ( $I_{d-p}$ ) as:

$$MTF = \sqrt{FT(I_{d-p})}$$

where FT indicates Fourier Transform.

The conventional configuration with equal size entrance and exit pupils produces even symmetric images and, therefore, all phase information is lost (Artal *et al.*, 1995a). Modifying the system to use unequal entrance and exit pupil sizes (with

one of them being small enough to produce a diffraction-limited retinal image) retains information on the actual shape of the PSF. With computational phase retrieval techniques, the ocular PSF, and subsequently the wave aberration, can be reconstructed from a pair of double-pass images (Artal *et al.*, 1988; Iglesias *et al.*, 1998). This reconstruction constitutes a phase retrieval problem similar to those found in astronomy.

## 2.2. Smirnov technique

The Smirnov technique consists of measuring local wavefront distortions through a series of small regions that span the optical zone of the cornea. Scheiner used

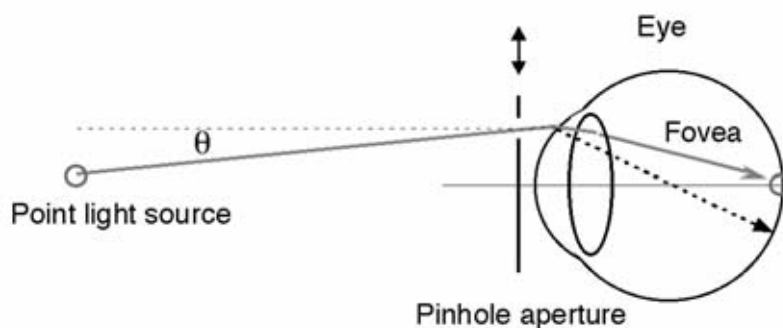


Figure 6. Smirnov technique.

a mask with two apertures in front of the eye to choose an appropriate spectacle correction (if the eye is ametropic, a double spot is created on the retina). The procedure was expanded upon by several researchers. Ivanoff (1953) directed two beams of light at the eye: one along the line of sight, and the other through different points on the eye's pupil. Each beam gave the image of a vertical line on the retina. The angle between the beams for which the subject sees both lines being coincident gives a measure of the lateral aberration. Smirnov (1962), inspired by this technique, used an adjustable aperture to image a crosshair on the retina. Changing the location of the aperture caused a corresponding shift in the location of the crosshair on the retina, shown in Fig. 6. The subject's task was to align the crosshair on the fovea by changing the angle of the incident light on the aperture. The wave aberration is calculated at this location based on this angle, and the crosshair is moved to a new position. Webb *et al.* (1992) devised a spatially resolved refractometer that incorporates two apertures, one being coincident with the corneal apex and the other having a variable position. The subject sees a reference image through the first aperture and the test image through the second and must align the test with the reference. Small angular displacements indicate a low amount of aberration whereas large angular displacements indicate the presence of large amounts of aberration.

### 2.3. Interferometric methods

With interferometry, one can introduce high frequency, high contrast interference fringes onto the retina (Campbell & Green 1965; Williams, 1985). Fig. 7 illustrates this method. Two coherent light beams sent through the eye's pupil

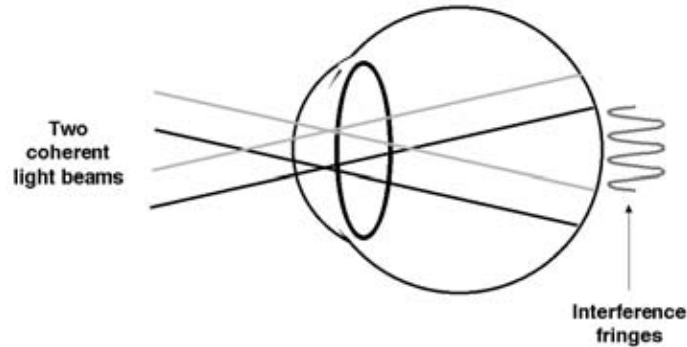


Figure 7. Two coherent beams form an interference fringe on the retina.

form an interference fringe on the retina, unaffected by the aberrations inherent in the eye's optics. The spatial frequency of the interference fringe is proportional to the separation of the point sources in the entrance pupil. The contrast is modified by the time that the pairs of light beams overlap. The contrast sensitivity of the visual system to interference fringes provides a lower estimate of visual performance than the contrast sensitivity of the retina and the brain alone (neural contrast sensitivity), because interference fringes are immune to most sources of optical blurring in the eye. The MTF of the eye can be estimated from the ratio between the contrast sensitivity function (CSF) to conventional gratings including the deleterious effects of the eye's aberrations and the CSF to interference fringes, or neural CSF (Campbell and Green, 1965; Williams *et al.*, 1994).

### 2.4. The aberroscope

Tscherning (1894) used an instrument to subjectively measure the aberrations of the eye when a subject viewed a light source through +5 D spherical lens and described the appearance of a square grid projected on the retina (Fig. 8). Howland and Howland (1977) designed an aberroscope similar to that of Tscherning but using  $\pm 5$  D crossed cylindrical lenses oriented with their axes at 45 degrees to the principal axes of an intercalated grid. An aberration-free eye receives an undistorted, square, shadow image of the grid upon its retina. Aberrations cause the image of the grid to be distorted. The subject then draws the perceived appearance of the grid to reproduce the distortions that he observed. From the resultant drawings the wave aberration is reconstructed. Walsh *et al.* (1984) modified Howland and Howland's subjective cross-cylinder aberroscope by adding a camera that directly photographed the distorted grid on the subject's retina, eliminating any subjective errors introduced by drawing the appearance of the aberrated grid.

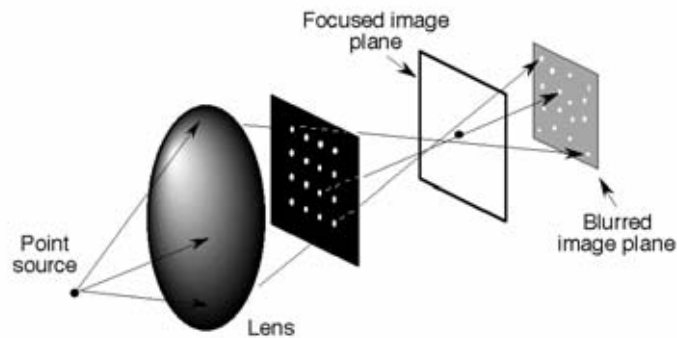


Figure 8. Aberroscope principle. Without aberrations, the array of point images matches the array of pinhole apertures. With aberrations (as illustrated in the figure), the displacement of point images from their reference position is a measure of the degree of aberration.

### 3. Hartmann-Shack Wavefront Sensor for the Eye.

The Hartmann-Shack (H-S) wavefront sensor is based on the Hartmann-Shack principle and was first applied as a tool to measure the eye's aberrations by Liang *et al.* in 1994. The method is fast, accurate, repeatable, and consistent with aberration measurements obtained using other techniques (Liang & Williams, 1997; Salmon *et al.*, 1998; Navarro *et al.*, 2000; Prieto *et al.*, 2000).

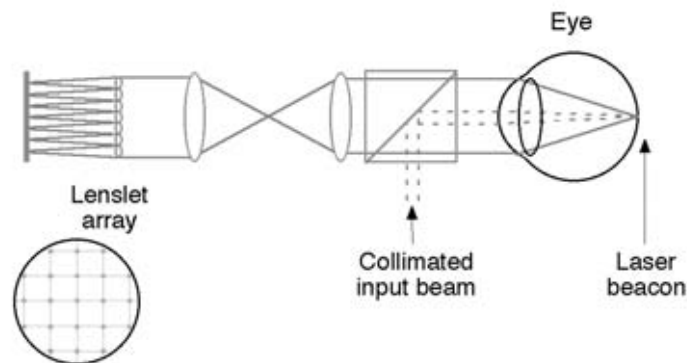


Figure 9. Hartmann-Shack wavefront sensor principle. A perfect eye would produce the spot array pattern shown in the figure, with all spots being equally spaced and symmetric.

The basic concept of the H-S sensor is illustrated in Fig. 9. Light from a laser, laser diode or superluminescent diode produces a compact point source on the retina that acts as a laser beacon. This light is then reflected by the retina and fills the entire pupil. If the eye has aberrations, the wavefront of

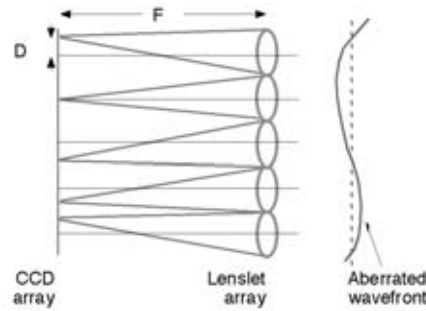


Figure 10. Hartmann-Shack lenslet array. Displacements,  $D$ , are proportional to the local wavefront slope at each lenslet.

the light exiting the pupil will be distorted from its ideal, planar form. This wavefront is replicated by the lenses at the plane of the lenslet array. The two-dimensional lenslet array samples this aberrated wavefront and forms an array of focused spots on a CCD array. The location of each spot relative to its ideal, on-axis location may be determined, with the degree of displacement of an individual spot being proportional to the local slope of the wavefront at that particular lenslet, shown in Fig. 10. The wave aberration may then be calculated from these series of local slopes at each lenslet across the eye's pupil. Typical parameters of a H-S sensor for the eye are listed below:

- Number of lenslets:  $\sim 200$ .
- Lenslet array: focal length = 24 mm.
- Lenslet diameter = 400  $\mu\text{m}$ .
- Number of CCD pixels per spot core: 5 to 14.
- Wavelength: 633 to 850 nm.

Fig. 11 shows an example of a H-S spot array pattern in an eye with the eyelid wide open and with the eyelid in its normal position. This subject's eyelid pulled so tightly across their cornea that it permanently altered their corneal shape. The Hartmann-Shack wavefront sensor is an excellent tool that can be used to observe irregularities in the eye's optics.

The effect of aberrations on a typical human eye can be seen in Fig. 12. The array of H-S spots for the eye is irregular, especially at the periphery of the pupil. This is also illustrated by the pictures comparing the wave aberration of a perfect eye to that of a normal, aberrated eye. The higher density of contour lines at the edge of the pupil indicates that the aberrations are becoming more severe.

The wave aberration calculated from the spot displacements in the H-S images is usually described using Zernike polynomials. The Zernike base has desirable mathematical properties over circular pupils and is therefore a useful base for

representing the eye's aberrations. Zernike polynomials are orthogonal, represent balanced aberrations, and can also be related to the classical Seidel aberrations. Fig. 13 shows a scheme for calculating Zernike coefficients from the local slopes of the H-S spots.

Second order Zernike polynomials contain one defocus and two astigmatic modes. Third order aberrations includes coma and triangular astigmatism. Spherical aberration is an example of a fourth order Zernike mode. Each Zernike coefficient indicates the magnitude of a particular aberration. A measure of the total amount of aberration in the eye is the root-mean-square (RMS) of the wave aberration, which can be easily calculated from the Zernike coefficients as the square root of the sum of the squares of all Zernike coefficients.

## 4. Properties of the Eye Important for Wavefront Sensor Design

### 4.1. Corneal reflection

A considerable fraction of the light incident on the eye is reflected by the cornea. Approximately 2.3% of the input light entering the H-S sensor is reflected from the cornea, while only about 0.01% is reflected from the retina. The corneal reflection is therefore 20-2000 times brighter than the retinal reflection, seeming to indicate that it would be extremely difficult to obtain H-S measurements.

Three methods can be used to avoid the corneal reflection:

1. Place a pinhole between the two relay lenses in Fig. 9. In this plane (which is conjugate with the retina) the light coming from the cornea is completely defocused and will be blocked by the pinhole. However, a potential problem with this method is that, for large aberrations, the light coming from the retinal beacon will not tightly focus at the center of the pinhole. In this case, the pinhole will also throw away important information concerning the aberration structure of the eye.
2. Use a polarized input beam along with a polarizing beam splitter. Light reflected by the cornea maintains its polarization and would be reflected by the polarizing beamsplitter. The depolarized light from the retina would be transmitted by the polarizing beamsplitter and sent towards the lenslet array. However, a small portion of the retinal reflection also maintains its polarization and would be lost as it is reflected by the beamsplitter. In addition, due to the birefringence of the cornea, only certain areas of the corneal reflection would be avoided, producing a non-uniform intensity distribution of the spots on the CCD array.
3. Use an off-axis input beam. This assures that the corneal reflection takes place in an oblique direction and does not propagate through the H-S sensor. If the angle of incidence of the input beam is only slightly off-axis, the beacon will still be formed on the fovea with no consequences for wave aberration measurement.

### 4.2. Image speckle

A second factor that affects the H-S sensor is speckle present in the image of the H-S spots. Speckle can reduce the accuracy of determining the exact centers of

each spot. There are two main procedures that can be used to reduce coherence and avoid speckle:

1. Let retinal motion decorrelate speckle. The necessary exposure time varies for different light sources. For a polarized laser, the exposure time should be greater than 500 ms. For an unpolarized laser, the duration of the exposure should be longer than 200 ms, while the exposure time for an unpolarized superluminescent diode can be as low as 30-50 msec due to its short coherence length.
2. Scan the beam across a small portion of the retina while taking the measurement to average out the speckle (Hofer *et al.*, 1999). This technique is more complex since it requires a motorized scanning mirror.

### 4.3. Spectral considerations

How much light makes it to the retina? The transmittance curve, shown in Fig. 14, indicates that the wavelength of the light source may be chosen from a broad spectral range that has a fairly uniform transmission spectrum. However, the same figure also shows that retinal reflectance increases with increasing wavelength, implying that more light will be reflected from the retina if a longer wavelength is chosen. A good light source for wavefront sensing is a superluminescent diode (SLD) that operates at 780 nm. A SLD that operates in the near infrared provides a comfortable, low coherence viewing source, rendering H-S images that are relatively speckle-free.

### 4.4. Laser safety for intrabeam viewing

How much light can safely enter the eye? According to the American National Standard for the Safe Use of Lasers (ANSI, 1993), the maximum permissible exposure (MPE) for a given exposure time,  $t$ , is:

Wavelength ( $\mu\text{m}$ )	Exposure, $t$ (sec)	MPE (joules)
0.4-0.7	$18 * 10^{-6}$ to 10	$0.0006927 t^{3/4}$
0.7-1.05	$18 * 10^{-6}$ to $10^3$	$0.0006927 t^{2(\lambda-0.7)}$

For example, the maximum power safely allowed for a 1/4 sec exposure would be 1 mW (245  $\mu\text{J}$ ) for 700 nm, or 2.2 mW (555  $\mu\text{J}$ ) for 780 nm. A typical H-S sensor for the eye operates at 10  $\mu\text{W}$  for a 200 msec exposure at 633 nm. This is equivalent to 2  $\mu\text{J}$  of power, which is much lower (a factor of 100 less) than the MPE of 207  $\mu\text{J}$ .

The MPE set by the ANSI standards is one order of magnitude below the power that would damage the eye. Hence, the H-S exposure is 3 orders of magnitude below the limit that could induce potential damage to the eye.

### 4.5. Pupil dilation and accommodation control

The diameter of the natural pupil is about 3-5 mm in normal illumination. If one wants to obtain wave aberration measurements for a larger pupil, it is often necessary to use a mydriatic agent to dilate the pupil. In addition, a cycloplegic agent may also be used to paralyze accommodation to avoid fluctuations in

focus. In addition, H-S sensor can work fast and track part of the remaining fluctuations. The following table lists the periods of mydriasis and cycloplegia obtained with two main drugs, tropicamide and cyclopentolate (Edgar, 1998). The average time window in which it is possible to obtain measurements under total mydriasis and cycloplegia is about 30 to 60 minutes.

Topical drug	Mydriasis	Cycloplegia
Tropicamide	30 min to >3 hr	15 min to 1 hr
Cyclopentolate	30 min to days	15 min to 2 hrs

#### 4.6. Chromatic aberration of the eye

In addition to the presence of monochromatic aberrations in the eye's optics, the human eye also suffers from chromatic aberration (Thibos *et al.*, 1990). The dispersion of the eye is practically the same as that of water. Shorter wavelengths focus before longer wavelengths, i.e., the eye is more myopic for blue light than for red light. There is little variation in chromatic aberration between different subjects. Fig. 15 shows a summary of the results from different researchers who examined the change in focus, or refractive error, of the eye for different wavelengths of light. Over the visible spectrum, there is nearly a 2.5 D change in the chromatic refractive error of the eye. Due to chromatic aberration, a H-S sensor operating in white light would produce a pattern of blurred spots.

#### 4.7. Spot quality in abnormal eyes

The measurement of the aberrations of abnormal eyes is fundamental for clinical applications. Two clinical conditions associated with abnormal eyes that are particularly important are anomalies of the tear film (dry eye) and corneal disease (keratoconus). In some of these cases, it is only possible to obtain partial information from H-S images (Fig. 16), resulting in the loss of wavefront information (Thibos & Hong, 1999).

Fig. 16 first compares the aberrations of an eye immediately after a blink (when the tear film is intact) and 40 sec later, after the tear film was disrupted by drying. This subject has unstable tears that begin to break up just a few seconds after each blink. It is clear from the image that the drying of the tear film produces a spot pattern that is difficult to analyze, but also indicates the efficacy of the H-S sensor to show the major impact of the dry film in the optical quality of these eyes.

The keratoconic cornea is another clinical condition in which the quality of the spots in the H-S images can be poor. Fig. 16 also shows the H-S data obtained from a keratoconic patient. The great distortion of the matrix of spots makes it difficult to analyze the aberrations of this eye.

### 5. Distribution of Aberrations in the Population

#### 5.1. Normal population measurements

Fig. 17 presents the magnitude of the monochromatic aberrations measured with a H-S wavefront sensor in a population of 109 normal subjects across a 5.7 mm pupil (Porter *et al.*, 2000a-b). The aberration with the largest magnitude is

defocus,  $Z_2^0$ , accounting for 80% of the variance of the wave aberration, followed by the two Zernike modes representing astigmatism,  $Z_2^{-2}$  and  $Z_2^2$ . The higher order aberrations account for 7% of the total variance. However, these higher order aberrations play a significant role in affecting retinal image quality. In general, there is a tendency for the magnitude of the higher order aberrations to decrease with increasing order. The Zernike coefficients, with the exception of spherical aberration, had a mean value approximately zero. The mean value for spherical aberration in this population was  $-0.138 \pm 0.103 \mu\text{m}$  for the 5.7 mm pupil.

Understanding the distribution of the aberrations in the population of human eyes is important from both a fundamental and a clinical point of view. A statistical analysis of the wave aberrations measured in this large population showed enormous intersubject variability. There appears to be a random variation in the wave aberration from subject to subject (Porter *et al.*, 2000a-c). On the other hand, aberrations in the left eye have been found to be significantly correlated with their counterparts in the right eye (Porter *et al.*, 2000a-c), indicating mirror-like symmetry in the wave aberration between eyes within an individual. A study is also being conducted to characterize the phase structure function across the eye's pupil and explore the possibility of a Fried's parameter for the eye (Zhao *et al.*, 2000).

## 5.2. LASIK subjects

The H-S sensor is also a valuable instrument for measuring the wave aberration of subjects after laser refractive surgery. Current surgical procedures introduce higher order aberrations that are not present in the pre-operative eye (Fig. 18). The increase in aberration structure occurs mainly at the pupil edge due to a steepening of the cornea near the transition zone of the ablation (Oshika *et al.*, 1999). This primarily produces an increase in spherical aberration (a fourth order Zernike mode), although other higher order aberrations such as coma also increase after surgery (Williams *et al.*, 2000). Wavefront sensing is becoming a key component that will be instrumental in perfecting laser refractive surgical techniques.

## References

- American National Standard for the Safe Use of Lasers, 1993, ANSI Z136.1-1993, (Laser Institute of America, Orlando, FL).
- Artal, P., Marcos, S., Navarro, R., & Williams, D. R., 1995a, *J. Opt. Soc. Am. A*, 12, 195.
- Artal, P., Iglesias, I., Lopez-Gil, N., & Green, D. G., 1995b, *J. Opt. Soc. Am. A*, 12, 2358.
- Artal, P., Santamaria, J., & Bescos, J., 1988, *J. Opt. Soc. Am. A*, 5, 1201.
- Campbell, F. W., & Green, D. G., 1965, *J. Physiol.*, 1981, 576.
- Campbell, F. W., & Gubisch, R. W., 1966, *J. Physiol.*, 186, 558.
- Charman, W. N., 1983, in *Progress in retinal research*, ed. Osborne, N., & Chader, G., (Pergamon Press, Oxford), vol. 2, chap. 1.

- Edgar, D. F., 1998, *Ophthalmic Physiol. Opt.*, 18, 97.
- Flamant, F., 1955, *Revue d'Optique*, 433.
- Guirao, A., Gonzalez, C., Redondo, M., Geraghty, E., Norrby, S., & Artal, P., 1999, *Inv. Ophth. Vis. Sci.*, 40, 203.
- Guirao, A., & Artal, P., 1999, *Vision Res.*, 39, 207.
- Helmholtz, von H., 1962, in *Popular Scientific Lectures*, ed. M. Kline (Dover, New York).
- Helmholtz, von H., 1896, *Physiological Optics*, J. P. C. Southall ed. (Dover, New York).
- Hofer, H., Artal, P., Aragon, J. L., & Williams, D. R., 1999, *Inv. Ophthal. Sci. Suppl.*, 40, S365.
- Howland, H. C., & Howland, B., 1977, *J. Opt. Soc. Am.*, 67, 1508.
- Iglesias, I., Lopez-Gil, N., & Artal, P., 1998, *J. Opt. Soc. Am. A*, 15, 326.
- Ivanoff, A., 1953, *J. Opt. Soc. Am.*, 46, 901.
- Liang, J., Grimm, B., Goelz, S., & Bille, J. F., 1994, *J. Opt. Soc. Am. A*, 11, 1949.
- Liang, J., & Williams, D. R., 1997, *J. Opt. Soc. Am. A*, 14, 2873.
- Lopez-Gil, N., Iglesias, I., & Artal, P., 1998, *Vision Res.*, 38, 2897.
- Miller, D. T., 2000, *Physics Today*, January, 31.
- Navarro, R., Artal, P., & Williams, D. R., 1993, *J. Opt. Soc. Am. A*, 10, 201.
- Navarro, R., Moreno-Barriuso, E., Marcos, S., & Burns S.A., 2000, *Invest. Ophthalm. Vis. Sci.*, 41, S427.
- Oshika, T., Klyce, S.D., Applegate, R.A., Howland, H.C., & El Danasoury, M.A., 1999, *Arch. Ophthalmol* 127, 1.
- Porter, J., Guirao, A., Williams, D.R. & Cox, I., 2000a, In: *Vision Science and Its Applications*. OSA Technical Digest. Washington DC, PD4-1.
- Porter, J., Cox, I.G., Guirao, A., Potvin, R.J., Lagana, M.A., & Williams, D. R., 2000b, *Invest. Ophthalm. Vis. Sci.*, 41, S428.
- Porter, J., Guirao, A., Cox, I.G., & Williams, D.R., 2000c, *J. Opt. Soc. Am. A*, (submitted).
- Prieto, P. M., Vargas-Martin, F., Goelz, S., & Artal, P., 2000, *J. Opt. Soc. Am. A*, 17, 1388.
- Salmon, T. O., Thibos, L. N., & Bradley, A., 1998, *J. Opt. Soc. Am. A*, 15, 2457.
- Santamaría, J., Artal, P. & Bescós, J., 1987, *J. Opt. Soc. Am. A*, 4, 1109.
- Smirnov, A., 1962, *Biophysics*, 6, 766.
- Thibos, L. N., Bradley, A., Still, D. L., Zhang, X., & Howarth, P. A., 1990, *Vision Res.*, 30, 33.
- Thibos, L. N., & Hong, X., 1999, *Optom. Vis. Sci.*, 76, 817.
- Tscherning, M., 1894, *Z. Psychol. Physiol. Sinn.*, 6, 456.
- Walsh, G., Charman, W. N., & Howland, H. C., 1984, *J. Opt. Soc. Am.*, 1, 987.
- Webb, R. H., Penney, C. M., & Thompson, K. P., 1992, *Applied Optics*, 31, 3678.

Williams, D. R., 1985, *Vision Res.*, 25, 195.

Williams, D. R., Brainard, D. H., McMahon, M. J., & Navarro, R., 1994, *J. Opt. Soc. Am.*, 11, 3123.

Williams, D. R., Artal, P., Navarro, R., McMahon, M. J., & Brainard, D. H., 1996, *Vision Res.*, 36, 1103.

Williams, D. R., Yoon, G.Y., Porter, J., Guirao, A., Hofer, H., & Cox, I., 2000, *J. Refrac. Surgery*, 16, 1.

Zhao, H., Miller, D. T., Thibos, L. N., Hong, X., Bradley, A., Cheng, X., & Himebaugh, N., 2000, OSA Annual Meeting, talk WO3.

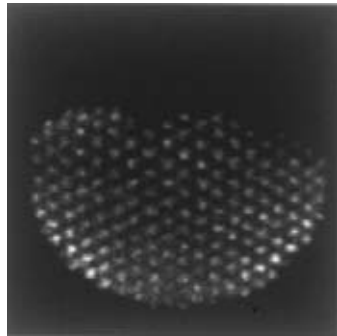


Figure 11. Hartmann-Shack spot array pattern from the same eye with the eyelid wide open (left) and the eyelid in its normal position (right).

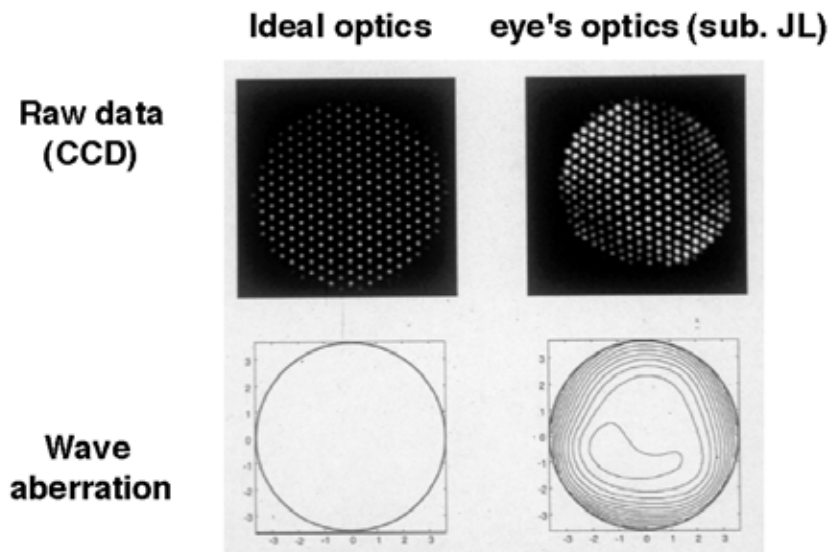


Figure 12. Hartmann-Shack spot arrays for an ideal eye with no aberrations (left) and a normal eye (right) across a 6 mm pupil. Also shown are the associated wave aberrations calculated from the spot patterns (each contour line is 0.15 microns).

$$[S] = \begin{bmatrix} \frac{\partial Z}{\partial x, y} \end{bmatrix} [C]$$

Slope measurement [m,1]      Partial derivatives of Zernike polynomials [m,n]      Zernike coefficients [n,1]

$$[C] = \left( \frac{\partial Z}{\partial x, y} \right)^T \frac{\partial Z}{\partial x, y} \text{ }^{-1} \frac{\partial Z}{\partial x, y} \text{ }^T [S]$$

Zernike coefficients      Least squares solution to inverse      Slope measurement

Figure 13. Determination of  $n$  Zernike coefficients,  $C$ , from a vector of  $m$  slopes by means of a least square inversion.

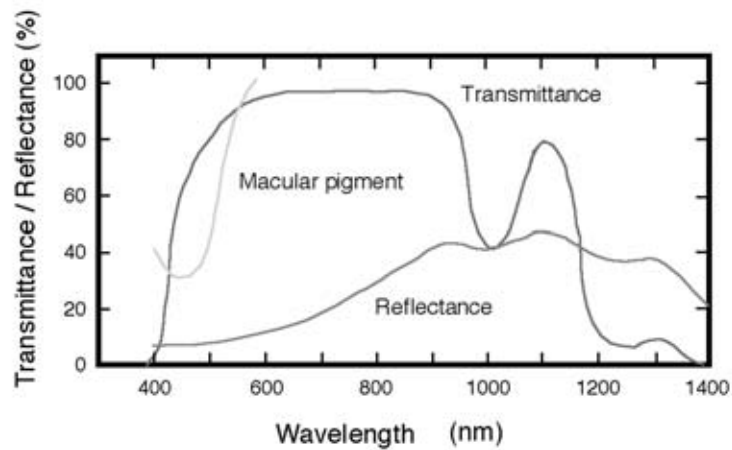


Figure 14. Transmittance and reflectance curves for the human eye.

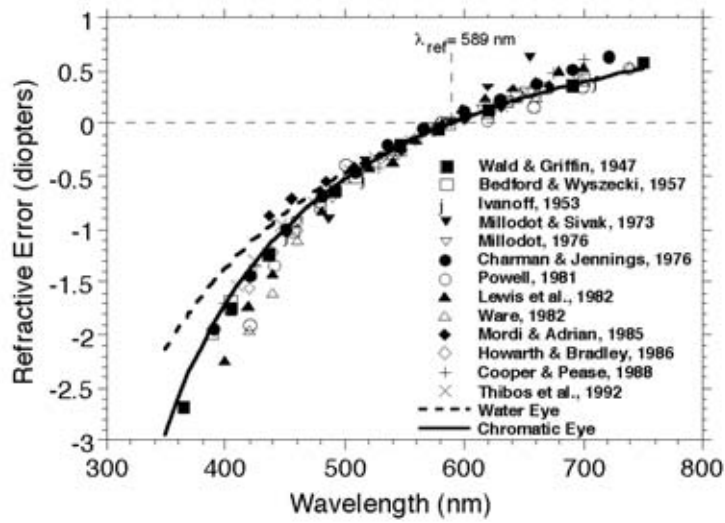


Figure 15. Chromatic difference of focus in the eye as a function of wavelength from several studies.

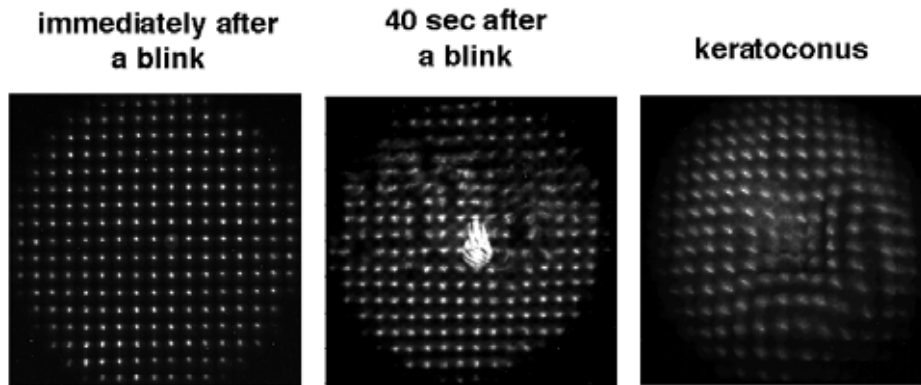


Figure 16. Optical effects of tear film disruption and a keratoconic cornea on the spot pattern. (Thibos & Hong, 1999).

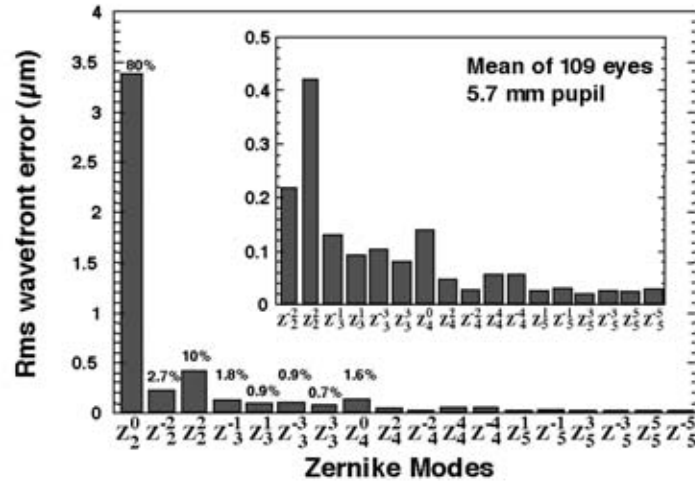


Figure 17. Mean absolute root-mean-square (RMS) values for Zernike modes up to fifth order measured from a population of 109 normal human subjects across a 5.7 mm pupil. Subjects aged between 21 and 65 years. Percentages labeled above the first eight modes designate the percent of the variance accounted for by each mode. (Porter *et al.*, 2000c).

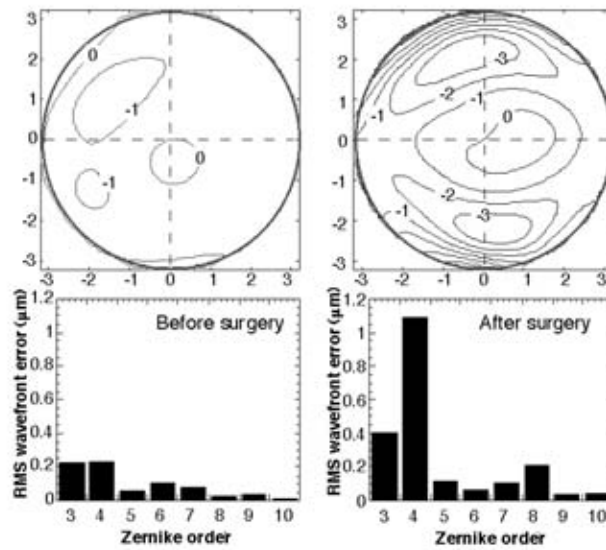


Figure 18. Wave aberration map in a normal eye the day before laser refractive surgery (LASIK) and in the same eye the day after surgery. Also shown is the magnitude of the aberrations for different Zernike orders. [Thibos & Hong, 1999].